Geometric Effects on the Acceleration Mechanisms in Applied-Field Magnetoplasmadynamic Thrusters

IEPC-2013-115

Presented at the 33rd International Electric Propulsion Conference,
The George Washington University • Washington, D.C. • USA
October 6 – 10, 2013

Meng-Di Kong[1] and Hai-Bin Tang[2]
Beihang University, Beijing, 100191, China

Abstract: Two applied-field magnetoplasmadynamic (AF-MPD) thrusters that are of different anode radii and had been investigated experimentally by the NASA Lewis Research Center Group have been simulated with the particle-in-cell with Monte Carlo collision (PIC-MCC) method to investigate the geometric effects on the acceleration mechanisms in AF-MPD thrusters. Specific impulse variations with different applied magnetic field strengths (0.034T-0.102T) were calculated and then used to verify the theoretical approach by comparing them with the experimental data. Following conclusions were obtained: (1) swirl acceleration mechanism was the dominant acceleration mode, and thrust proportions resulting from self-magnetic, Hall, gas-dynamic, and swirl acceleration mechanisms were in an approximate ratio of 1:10:10:100 for both thrusters; (2) total ion qualities in the thruster with smaller anode radius tended to be larger, and therefore the three electromagnetic acceleration mechanisms (except the gas-dynamic one) in it tended to work more effectively, whereas the gas-dynamic acceleration mechanism almost bore no relation to the anode radius under the given operation conditions; (3) anode shape may affect the gas-dynamic acceleration mechanism strongly and this effect will be included in future investigations to shed more light on the optimum geometry design of AF-MPD thrusters.

Nomenclature

$\boldsymbol{A}$	=	magnetic vector potential
$\boldsymbol{B}$	=	magnetic field, T
$\boldsymbol{E}$	=	electric field, V/m
e	=	elementary charge, C
I	=	discharge current, A
$\boldsymbol{j}$	=	current density, A/m^2
k	=	Boltzmann constant
m	=	particle mass, kg
$\dot{m}$	=	mass flow rate, kg/s
n	=	number density, /m^3
P	=	collision probability
Q_t	=	collision cross section, m^2
r	=	radical location, m
Δr	=	radical distance step, m
$\boldsymbol{s}$	=	location vector, m

[1] Master Candidate, School of Astronautics, kongmengdi@sa.buaa.edu.cn.
[2] Professor, School of Astronautics, thb@buaa.edu.cn.

$\boldsymbol{T}$	=	thrust, N
t	=	time, s
Δt	=	time step, s
$\boldsymbol{u}$	=	velocity, m/s
z	=	axial location, m
Δz	=	axial distance step, m
ϕ	=	plasma potential, V
ε_0	=	free-space permittivity
μ_0	=	permeability of free space, H/m
λ_D	=	Debye length, m

I. Introduction

Magnetoplasmadynamic (MPD) thrusters can achieve high exhaust velocities combined with high thrust densities by using Lorentz forces resulting from the interactions of currents and magnetic fields,[1] and are attractive candidates for propelling manned spacecraft to other planets. According to the source of the magnetic field, MPD thrusters can be divided into self-field MPD (SF-MPD) thrusters and applied-field MPD (AF-MPD) thrusters, and the latter are capable of achieving higher thrust efficiencies and more stable operations at high specific impulse with less electrode erosion.[2] There exist complex coupling of plasma heating, ionization, and acceleration phenomena in MPD thrusters, and thruster performance is strongly affected by operation conditions such as the discharge current, mass flow rate, applied magnetic field strength, and electrode geometry.[3] The main purpose of this work is to investigate the geometric effects on the acceleration mechanisms in AF-MPD thrusters and provide some insights into the optimum geometry design of AF-MPD thrusters under certain conditions.

Investigation of acceleration mechanisms is the foundation for optimum thruster design and there have been many studies about the acceleration processes in AF-MPD thrusters over the past 40 years, both experimentally and theoretically.[4] Four main acceleration mechanisms, i.e., self-magnetic, swirl, Hall, and gas dynamic acceleration have been identified for AF-MPD thrusters, and the relative importance of each other may vary with operation conditions, whereas the dominant mechanism is still the subject of much debate.[5,6]

Myers[7] studied the effects of electrode geometry and applied magnetic field strength on the performance of a 100kW, steady-state, applied-field MPD thruster to establish its scaling law, and swirl acceleration was mainly dominant under the given operation conditions.

In a theoretical study of a 100 kW, steady-state, applied-field, argon MPD thruster, Tang et al. used the particle-in-cell (PIC) method to model the acceleration mechanisms in the thruster quantitatively.[4] They concluded that swirl acceleration mechanism was the dominant contributor to the plasma acceleration, while self-magnetic, Hall, gas dynamic, and swirl acceleration mechanisms were in an approximate ratio of 1:10:10:100.

Using a two-dimensional magnetohydrodynamics (MHD) code MACH2, Mikellides et al. conducted simulations of a 100-kW, steady-state, applied-field argon MPD thruster.[8] It was reported that their simulation results were in good agreement with those of the experiments, and gas dynamic acceleration was considered to be the dominant acceleration mode under their operation conditions.

Sasoh and Arakawa[9] investigated a steady-state AF-MPD thruster with hydrogen, helium, nitrogen, and argon at input power levels of 2-16kW, and derived a thrust formula which can roughly evaluate thrust components caused by swirl, Hall, and self-field accelerations. They concluded that Hall acceleration played an important role in thrust production at high applied field strengths and low mass flow rates, and the main acceleration mechanism may vary with operation conditions.

Besides the debates on the prevailing acceleration mode, almost all the previous studies on acceleration processes in AF-MPD thrusters[4-13] were only focused on only one kind of geometry, and therefore were not able to provide model predictions about the thruster geometry, which may have a notable influence on the acceleration mechanisms in the thruster. What's more, though there do exist many studies on the geometric effects of AF-MPD thrusters[14-19], most of the them were carried out experimentally and attempted to address the effects of thruster geometry on its macroscopic characteristics such as thrust, impulse or efficiency, instead of investigating the underlying and mostly microscopic acceleration mechanisms.

Performances of 100kW class, AF-MPD thrusters were evaluated by Mantenieks et al. and six thruster configurations were characterized as function of discharge current, mass flow rate, and applied magnetic field strength.[15] Thrust measurements were obtained with three of the thruster configurations and thrust was found to increase monotonically with the product of arc current and magnet current.

Myers et al. tested three AF-MPD thruster geometries with argon propellant to establish the influence of electrode geometry on thruster performance.[16] The results showed that thrust increased approximately linearly with anode radius, while the discharge and electrode fall voltages increased quadratically with anode radius. Thrust efficiency, on the other hand, was not significantly influenced by the changes in geometry over the operation range studied.

Eight AF-MPD thruster configurations were tested with argon propellant at power levels between 20-130kW by Myers to study the effects of geometry and applied magnetic field strength on thruster performance.[17] The results showed that both cathode radius and anode radius influenced the efficiency-specific impulse relationship fundamentally, whereas their lengths only influenced the magnitude of the applied magnetic field required to reach a given performance level. However, this study was not able to determine performance limits for these thrusters or established what geometries and operation conditions were associated with improved performance.

Takubo et al.[18]investigated the performance of the 2D AF-MPD thruster experimentally by using several inter-electrode geometry configurations and concluded that under an external magnetic field of 0.25 T and with the same anode and cathode radius, the shortest discharge chamber length led to the highest thrust.

Given the above clarifications, investigations considering the acceleration mechanisms and thruster geometry simultaneously are definitely needed. The goal of this study is to establish the effects of thruster geometry on the acceleration mechanisms in the thruster and shed some light on the design of more efficient AF-MPD thrusters. Based on the experimental investigations conducted by the NASA Lewis Research Center, this paper presents the results of a numerical study in which two AF-MPD thrusters with different anode radii were simulated across the same range of operation conditions. Besides, numerical simulations will be continued in the future to investigate the acceleration mechanisms in AF-MPD thrusters with different anode shapes, flared anode for instance, to get a deeper understanding of the geometric effects. The structure of this paper is as follows: Sec. II introduces the numerical method and algorithm; Sec. III describes the detailed analytical modeling processes; Section IV discusses the results obtained from present simulations; and Section V summarizes the study and presents some prospects.

II. Numerical Method and Algorithm

Investigations on AF-MPD thrusters have been conducted widely over the past several decades, and several numerical models have been established to investigate the coupling and complex physical processes in the thruster. Generally speaking, the simulation models can be divided into two categories, macroscopic models which are based on MHD equations and PIC models which are based on particle dynamics. In fact, macroscopic models based on MHD equations are frequently adopted in studies about MPD thrusters and several codes have been successfully developed to investigate the physical phenomena involved and improve experimental performance.[8,19-22] However, owing to the inherent assumptions and empirical parameters accompanying the continuum theory, and the species complexity of the AF-MPD thruster plasma flows, it's hard to obtain the exact transport coefficients of the flows and to evaluate their impacts on the results. Besides, MHD codes are not able to capture the microscopic phenomena and nonlocal dynamic effects of particles.

As an alternative and conventional way to investigate the physical processes of plasma flows, PIC method has been widely used in Hall and ion thruster modeling.[23-28] According to the difference in the way of dealing with electrons, the PIC method can be further classified into the hybrid-PIC method where electrons are treated as a fluid and the full PIC method where all particles including electrons are processed kinetically. As a good trade-off between the macroscopic and full PIC models, hybrid-PIC models can provide numerical solutions in relatively short time, despite the disparate dynamic scales of electrons and ions, and the relatively complex thruster geometry and magnetic field topology in Hall and ion thrusters.[29-31]However, the hybrid-PIC model becomes quite complicated when it comes to AF-MPD thrusters because many simplifying assumptions on the electron flows used in Hall or ion thruster modeling are not appropriate now, and the governing equations of electrons under three-dimensional modeling conditions are difficult to solve. Thus, an effective and simplified hybrid-PIC technique for studying AF-MPD thrusters is still a problem. The full PIC method, however, circumvents this problem by treating all the particles including electrons kinetically and has been successfully implemented in a recent study on AF-MPD thrusters.[4,32]

The full PIC method is a direct simulation technique where neutrals, ions, and electrons are treated as discrete particles. Macroscopic electromagnetic fields are obtained by solving Poisson's equation and Maxwell's equations, and Newton's second law is used to get individual particle's positions and trajectories. The general equations are as follows:

$$\nabla^2\phi = -\frac{e}{\varepsilon_0}\left(n_i - n_e\right), \tag{1}$$

$$\boldsymbol{E} = -\nabla\phi, \tag{2}$$

$$\nabla \times \boldsymbol{B} = \mu_0 \boldsymbol{j}, \tag{3}$$

$$\nabla \cdot \boldsymbol{B} = 0, \tag{4}$$

$$m\frac{d\boldsymbol{u}}{dt} = e\left(\boldsymbol{u} \times \boldsymbol{B} + \boldsymbol{E}\right), \frac{d\boldsymbol{s}}{dt} = \boldsymbol{u}. \tag{5}$$

Besides, to use the full PIC method, the simulation region should be divided into small grids with sizes smaller than the electron Debye length, and the calculation should be implemented on a time-step that is on the order of the inverse plasma time to capture electron dynamics. As a result, it would take millions of time-steps for neutrals and ions to cross the simulation region in a common AF-MPD thruster, that is, we'll have to track billions of particles for millions of time-steps in this case, which is far beyond the capabilities of current workstations. In order to make the simulation feasible on an ordinary workstation, some accepted and reasonable methods that have been successfully employed and tested in previous studies on Hall thrusters,[33] ion thrusters[26]and a recent study on AF-MPD thrusters[4,32]will be used here to speed up the calculation. The aforementioned techniques include: (1) using super-particles (groups of particles) in place of individual particles; (2) decreasing the mass of heavy particles to speed up convergence; (3) increasing the free-space permittivity constant to increase Debye length and reduce the grid density. There is no doubt that some parameters will be influenced by the application of these techniques during the iteration processes, but the effects will be under control and the main physical characteristics of plasmas will still be able to recover if corresponding theoretical adjustments are implemented, which has been elaborated in both Tang's and Szabo's studies.[32,33]

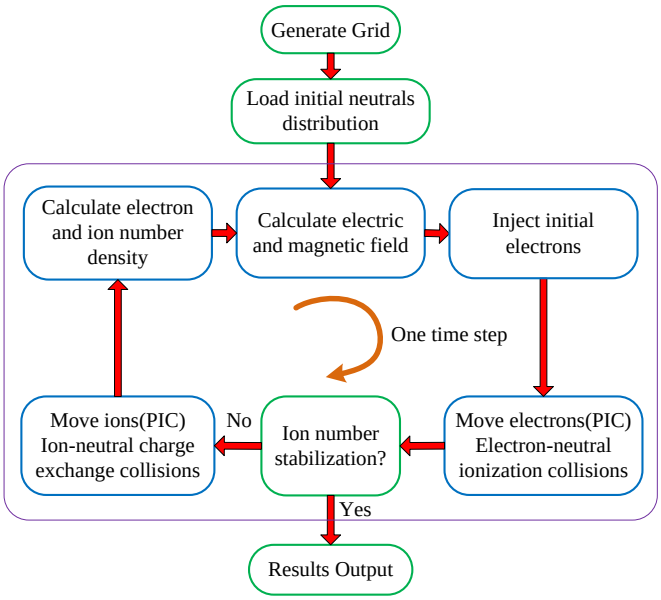

Figure 1. Schematic of the PIC-MCC numerical algorithm.

Moreover, to study the collisional effects among particles, a standard Monte Carlo Collision (MCC) approach will be used. In other words, the collisional probability of each charged particle will be tracked and the probability that a charged particle undergoes a collision within time t can be given by

$$P(t) = 1 - \exp(-\int_0^t nV_r Q_t dt), \tag{6}$$

where n is the background particle density, V_r is relative velocity of the two particles, and Q_t is the cross section for the interaction. Therefore, the collisional probability for each particle over each time step can be calculated by

$$P(t) = 1 - \exp(-nV_r Q_t \Delta t). \tag{7}$$

The probability will then be compared to a random number to determine whether a collision event takes place.[34]

Specifically, the detailed numerical algorithm of the PIC method used in the modeling of AF-MPD thrusters can be described as follows: first, the simulation region is divided into small grids; second, some guesses on particles' initial locations and velocities are made; third, an iterative technique is adopted in the calculation process. Moreover, during each time step of the iteration, the macroscopic electromagnetic fields on each node are computed or updated and weighted to particles inside the cell; next, new positions and velocities of particles are obtained by solving the particle equations of motion independently; then, conditions for collisions are checked to determine whether a certain collision occurs or not; furthermore, particle charge and density on each node are captured by using the new particle positions and velocities and a weighting scheme;[32] finally, the ion number density is checked to judge whether the expected stable state has been attained. Fig.1 presents the schematic of the PIC-MCC (particle-in-cell with Monte Carlo collision) numerical algorithm used.

III. Analytical Modeling

A. Acceleration Model and Thrust Evaluation

The AF-MPD thruster is a hybrid accelerator with electromagnetic and gas dynamic processes both contributing markedly to the acceleration of the propellant, and four main acceleration mechanisms have been identified in the thruster.[4,6,10] Fig.2 illustrates the four acceleration modes, which can be described as follows:

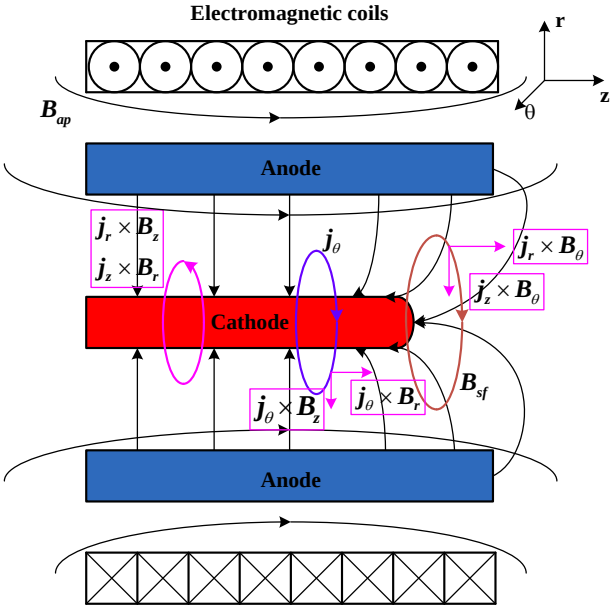

Figure 2. Schematic of the electromagnetic mechanisms in AF-MPD thrusters.

(1) Self-magnetic acceleration: The discharge current (with two components, $\boldsymbol{j}_r$ and $\boldsymbol{j}_z$) interacts with the azimuthal magnetic field $\boldsymbol{B}_\theta$ induced by the current flow, thus producing an electromagnetic force $\boldsymbol{j}_r \times \boldsymbol{B}_\theta$ in the axially outward direction and $\boldsymbol{j}_z \times \boldsymbol{B}_\theta$ in the radially inward direction. The axial component contributes to the thrust directly whereas the radial component adds to the thrust indirectly.

(2) Swirl acceleration: The interactions of discharge current ($\boldsymbol{j}_r$, $\boldsymbol{j}_z$) and applied magnetic field (with two components, $\boldsymbol{B}_z$ and $\boldsymbol{B}_r$) give rise to the azimuthal Lorentz force ($\boldsymbol{j}_r \times \boldsymbol{B}_z$ and $\boldsymbol{j}_z \times \boldsymbol{B}_r$), which tends to turn the plasma into rotation and impart rotational kinetic energy to it. Besides, the assumption that the rotational kinetic energy can be converted into the axial one through expansions in a physical or magnetic nozzle was the basis for the previous theoretical efforts.

(3) Hall acceleration: The azimuthal current $\boldsymbol{j}_\theta$ induced mainly by Hall effects interacts with the applied magnetic field ($\boldsymbol{B}_z$, $\boldsymbol{B}_r$), thereby producing electromagnetic force components $\boldsymbol{j}_\theta \times \boldsymbol{B}_z$ in the radial direction and $\boldsymbol{j}_\theta \times \boldsymbol{B}_r$ in the axial direction, whereas the directions of the force components (positive or negative contribution to the thrust) is still not clear.

(4) Gas dynamic acceleration: In this mode, the working plasma is heated up by Joule heating and then expands in a physical or magnetic nozzle, which is similar to the acceleration process that occurs in an electro-thermal arcjet. Furthermore, the additional gas dynamic thrust is associated with plasma pressure and this acceleration mechanism was still included in this study out of the consideration of practice though it is not classified as part of the electromagnetic acceleration.

In the AF-MPD thruster, dedicated thrust portions are attributed to different acceleration mechanisms, thus offering a way to evaluate thrust. Specifically, the self-magnetic thrust component attributed to the self-magnetic acceleration is summarized as T_{self}; the thrust component produced by the conversion of swirl motion is designated as T_{swirl}; thrust production originates from the azimuthal current is called T_{hall}; and the remaining axial pressure

component exerted on the nozzle is termed as T_{gd}. Then, with the assumption that the rotational energy is converted completely to the axial kinetic energy, the total thrust of an AF-MPD thruster can be evaluated as

$$T_{total} = T_{self} + T_{swirl} + T_{hall} + T_{gd}. \tag{8}$$

To quantitatively compute each acceleration mode and further determine the geometric effects on the acceleration mechanisms in the thruster, the aforementioned PIC-MCC method was used in this study. As shown in Fig.3, the assumed axisymmetric discharge region is surrounded by an anode and a cathode. Besides, under the cylindrical coordinates, the electric field $\boldsymbol{E}$, magnetic field $\boldsymbol{B}$, plasma velocity $\boldsymbol{u}$, and current density $\boldsymbol{j}$ are assumed to have following components respectively:

$$\boldsymbol{E} = \begin{bmatrix} E_z \\ E_r \\ 0 \end{bmatrix}, \ \boldsymbol{B} = \begin{bmatrix} B_z \\ B_r \\ B_\theta \end{bmatrix}, \quad \boldsymbol{j} = \begin{bmatrix} j_z \\ j_r \\ j_\theta \end{bmatrix}, \ \boldsymbol{u} = \begin{bmatrix} u_z \\ u_r \\ u_\theta \end{bmatrix}. \tag{9}$$

In practice, the electromagnetic field equations are solved by a finite-difference technique, where the particle number densities involved are determined by the PIC method. Combining the Poisson's equation (1) and a five-point scheme for finite differences based on axisymmetric coordinates, the electric potential can be found as

$$\frac{\phi_{i,j+1} - 2\phi_{i,j} + \phi_{i,j-1}}{\Delta r^2} + \frac{1}{r}\frac{\phi_{i,j+1} - \phi_{i,j-1}}{2\Delta r} + \frac{\phi_{i+1,j} - 2\phi_{i,j} + \phi_{i-1,j}}{\Delta z^2} = -\frac{e}{\varepsilon_0}\left(n_i - n_e\right). \tag{10}$$

According to Eq. (2) and a two-point scheme, the value of the two dimensional electric field on each node is then calculated, which can be given by

$$E_z(i,j) = -\frac{\phi_{i+1,j} - \phi_{i-1,j}}{2(z_{i+1} - z_i)}, \tag{11}$$

$$E_r(i,j) = -\frac{\phi_{i,j+1} - \phi_{i,j-1}}{2(r_{j+1} - r_j)}. \tag{12}$$

As far as the AF-MPD thruster is considered, the applied magnetic field is static and has both radical and axial components. In addition, the azimuthal self-magnetic field induced by the discharge current is still taken into account though its strength is rather small when compared with the applied magnetic field strength because it is the source of the self-magnetic acceleration. To solve the magnetic field, the magnetic vector potential ($\boldsymbol{A}$) can be defined, which satisfies

$$\boldsymbol{B} = \nabla \times \boldsymbol{A}. \tag{13}$$

Substitute Eq. (13) into Eq. (3) and Eq. (4), one can then obtain the vector potential equation

$$\nabla^2 \boldsymbol{A} = -\mu_0 \boldsymbol{j}. \tag{14}$$

Therefore, the three components of the strength of the magnetic field can be obtained by

$$\begin{cases} \boldsymbol{B}_z = \boldsymbol{B}_{ap,z} + \dfrac{\boldsymbol{A}_\theta}{\boldsymbol{r}} + \dfrac{\partial \boldsymbol{A}_\theta}{\partial \boldsymbol{r}} \approx \boldsymbol{B}_{ap,z} \\ \boldsymbol{B}_r = \boldsymbol{B}_{ap,r} - \dfrac{\partial \boldsymbol{A}_\theta}{\partial \boldsymbol{z}} \approx \boldsymbol{B}_{ap,r} \\ \boldsymbol{B}_\theta = \dfrac{1}{\boldsymbol{r}}\dfrac{\partial \boldsymbol{A}_r}{\partial \boldsymbol{z}} - \dfrac{1}{\boldsymbol{r}}\dfrac{\partial \boldsymbol{A}_z}{\partial \boldsymbol{r}} \end{cases} . \tag{15}$$

In addition, only singly charged ions were considered in this simulation and the plasma current can be obtained by

$$\boldsymbol{j} = e(n_i \boldsymbol{u}_i - n_e \boldsymbol{u}_e). \tag{16}$$

In general, the directed electromagnetic kinetic energy produced by axial forces contributes directly to thrust, while a large fraction of the energies imparted by forces in other directions can be converted into axial energy through the expansion in a nozzle. Under the assumption that all types of nondirected energies can theoretically be converted into the useful axial kinetic energy in the mechanical or the magnetic nozzle, the thrust portion produced by each mechanism can be calculated as

$$T_{self} = \int_V \sqrt{\left(j_r B_\theta\right)^2 + \left(j_z B_\theta\right)^2}\, dV, \tag{17}$$

$$T_{swirl} = \int_V \left(-j_r B_z + j_z B_r\right) dV, \tag{18}$$

$$T_{hall} = \int_V \sqrt{\left(j_\theta B_r\right)^2 + \left(j_\theta B_z\right)^2}\, dV, \tag{19}$$

$$T_{gd} = \int_S \left(k n_i T_i + k n_e T_e + k n_a T_a\right) dS. \tag{20}$$

Besides, as an important performance parameter, the exit velocity (or specific impulse) can be obtained in the simulation process. The mean value of the exit velocity $\boldsymbol{u}_{exit}$ can be obtained from the statistics of the particle velocities and number densities at the exit, as

$$\boldsymbol{u}_{exit} = \left(\sum_{j=1}^{N_J} n_j \boldsymbol{u}_j\right) / \sum_{j=1}^{N_J} n_j, \tag{21}$$

where N_J is the number of nodes at the exit.

B. Simulation Model

The simulation was focused on the modeling of two steady-state AF-MPD thrusters which had been investigated experimentally by Myers.[14] Fig.3 presents a typical configuration of the two thrusters and their detailed dimensions can be found in Table 1. The two thrusters all consist of a cylindrical copper anode and a coaxial, 2% thoriated tungsten cathode. For each kind of thruster, the model assumes that argon propellant is injected from the boron nitride backplate at 0.1g/s and the total discharge current is 1000A. The applied magnetic field was produced by the external coils surrounding the thruster and one end

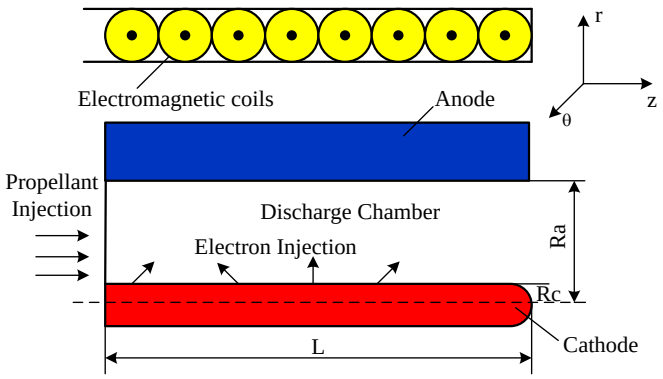

Figure 3. A typical AF-MPD thruster configuration.

of the magnet coil was flush with the exit plane. Moreover, two different coil sizes were employed to accommodate different thruster geometries and maximize the potential applied field. The first, with a bore diameter of 15.3 cm and a length of 15.3 cm, consisted of 36 turns of 1.3 cm diameter copper tubing, and was used for tests of geometry A; and the second, with a bore diameter of 20.3 cm and length of 15.3 cm, was made by using 28 turns of 1.9 cm diameter copper tubing, and was used for tests of geometry B. Besides, the applied magnetic field strengths were varied from 0.034 to 0.102 T by changing the coil currents for both thrusters.

Table 1. Dimensions of the two AF-MPD thrusters simulated.

Thruster Geometry	Anode Radius R_a (mm)	Cathode Radius R_c (mm)	Anode and cathode length L (mm)
A	25	6.4	76
B	51	6.4	76

Based on the characteristics of AF-MPD thrusters, the discharge chambers simulated were assumed to be axisymmetric in space and only electrons, single charged ions, and neutral atoms were taken into account. Atoms were taken as the background particles and the neutral particle temperature was assumed to be 500K while the initial velocity was under a Maxwellian distribution. As for the electrons, they were injected into the simulation region from the cathode surface under a quadratic distribution according to Ref.35, and the initial temperature was set to 0.2eV with a shifted Maxwellian distribution in velocity. Besides, each plasma component was assumed to be two dimensional in space (z, r) and three dimensional in velocity.

As for the boundary conditions, three types of boundaries were defined in the simulation model, i.e., free boundary, dielectric wall, and conductive wall. All particles are able to come across the free boundary, whereas dielectric or conductive walls are impenetrable and ions and electrons are neutralized there. In addition, the plasma potential boundaries on the anode and cathode in the simulation were set from the experimental data,[14] that is, the electric potential boundary conditions of the simulation model were the experimental discharge voltages minus the corresponding effective anode falls. Besides, the influence of the sheath on particle motions can be neglected in the current model since the sheath thickness is quite small when compared to the overall thruster dimensions. In fact, the sheath thickness is of the same order with Debye length, and can be calculated as

$$S = \frac{1}{\sqrt{\frac{n_e e^2}{\varepsilon_0 k T_e} + \frac{n_i e^2}{\varepsilon_0 k T_i}}} \approx \sqrt{\frac{\varepsilon_0 k T_e}{n_e e^2}} = \lambda_D . \tag{22}$$

Substitute the estimated plasma densities and temperatures of each thruster into Eq. (22), the relevant mean free paths of both thrusters can be obtained then, as shown in Table 2.

Table 2. Estimated values of parameters for the thrusters simulated.

Thruster Geometry	Electron density (m^{-3})	Electron temperature (eV)	Debye length (m)
A	5×10^{15}	1.0	1.0×10^{-4}
B	7×10^{14}	3.0	4.8×10^{-4}

Moreover, there exist various collisional processes in actual AF-MPD thrusters, but not all of them were included in the present model out of the consideration of simplifying calculations. In fact, whether a certain kind of collision should be taken into account depends on the corresponding mean free path and the collision's contributions to the physical processes in the thruster. The mean free path of a particle 1 interacting with a background of particle 2 is

$$\lambda_{12} = \frac{1}{Q_{12} n_2}, \tag{23}$$

where Q_{12} is the cross section for the interaction while n_2 is density of the background particles.

Given the estimated plasma number densities and temperatures, the mean free path of each kind of collision can be approximately evaluated, as presented in Table 3. Most of the mean free paths of particle collisions in the

simulation model far exceed the length of the simulation zone, so it is possible to neglect these collisions because of their infinitesimal effects on particle motions. However, the electron-atom ionization collision and the ion-atom exchange collision were still included in the present model since these two collisions can produce ions, which are essential for the thrust productions of AF-MPD thrusters. In addition, these two collisions can be modeled by the aforementioned Monte-Carlo method since the relevant mean free paths far exceed the grid size ($\Delta z = \Delta r = 1\times10^{-3}$ m).

Table 3. Mean free paths for various collisions in the channel of AF-MPD thrusters.

Collision pattern	Thruster A Mean free path (m)	Thruster B Mean free path (m)	Included
Electron-atom ionization collision	160	120	Y
Ion-atom exchange collision	140	150	Y
Electron-ion Coulomb collision	5	15	N
Electron-electron Coulomb collision	300	750	N
Atom-atom Coulomb collision	90	200	N
Ion-ion Coulomb collision	1500	16000	N

IV. Results and Discussion

A. Specific impulse variations with applied magnetic field strength

The specific impulse variations with applied magnetic field strengths of 0.034T, 0.052T, 0.085T and 0.102T for both thrusters under the mass flow rate $\dot{m} = 0.1$g/s and discharge current $I = 1000$A were obtained and then compared with the experimental data by using the PIC-MCC method, as illustrated in Fig.4. It shows that specific impulses vary linearly with applied magnetic field strengths and the simulation results are in good agreement with the experimental data, which can be taken as a basic verification of the validity of the model and the PIC-MCC method applied here.

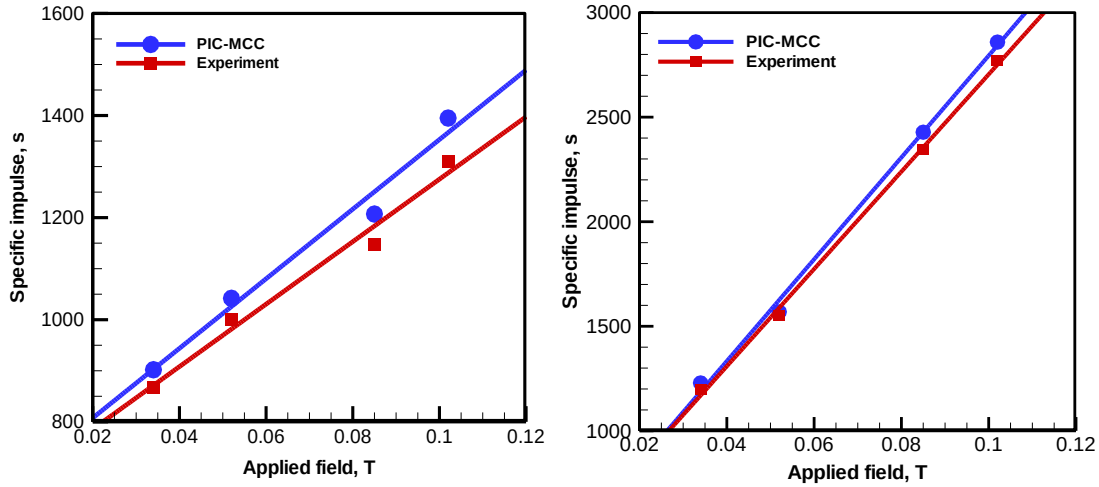

a) Thruster A **b) Thruster B**

Figure 4. Specific impulse variations with applied magnetic field strengths.

B. Magnetic field, particle density and current density distribution

To offer some insights into the microscopic features of AF-MPD thrusters and lay the foundations for the following analyses about acceleration mechanisms, the axial variations of the magnetic field, particle density and current density are presented and discussed here.

Fig.5 shows the variations of axial, radical and azimuthal magnetic field components with axial positions for different thruster geometries and various applied field strengths. Axial component is found to be the dominate one, whereas the self-induced azimuthal component is far less than the two applied components. Besides, a slowly diverging applied magnetic field is demonstrated, which is in accordance with the actual magnet designs of the two thrusters.

The variations of plasma density along the axial direction with various applied magnetic field strengths for the two thrusters are presented in Fig. 6. The plasma number densities decrease along the channel and with stronger applied magnetic field, the total quantities of the particles in the thruster will decrease, which implies that more charged particles are being accelerated and so leave from the exit boundaries. In addition, when comparing the plasma densities of the two thrusters, we can find the average density in thruster A (with a radius of 25mm) is about seven times of that in thruster B (with a radius of 51mm) at the same applied magnetic field strength though the volume ratio of the two thrusters is only about four, which implies the difference of the real ion quantities in the two thrusters. In other word, there exist more ions in the thruster with smaller anode radius, and may help to enhance the electromagnetic acceleration.

Fig.7 shows the variations of axial, radical and azimuthal current densities with axial positions for various applied field strengths. The radical component is much larger than the other two components, which means that the thrust component resulting from the radial current and axial magnetic field component is dominant in comparison with other Lorentz forces in the discharge chamber. Besides, the absolute value of the radical current density tends to increase and then decrease along the discharge channel, which may influence the axial distribution of the relevant swirl acceleration mechanism and will be discussed later.

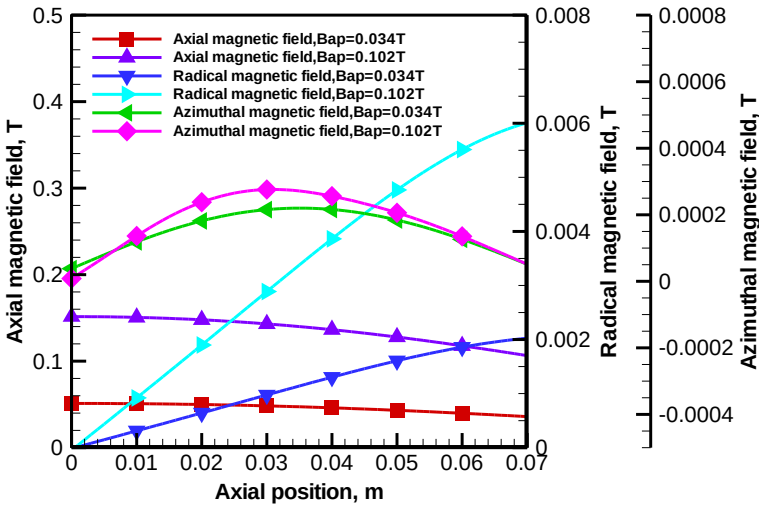

a) Thruster A

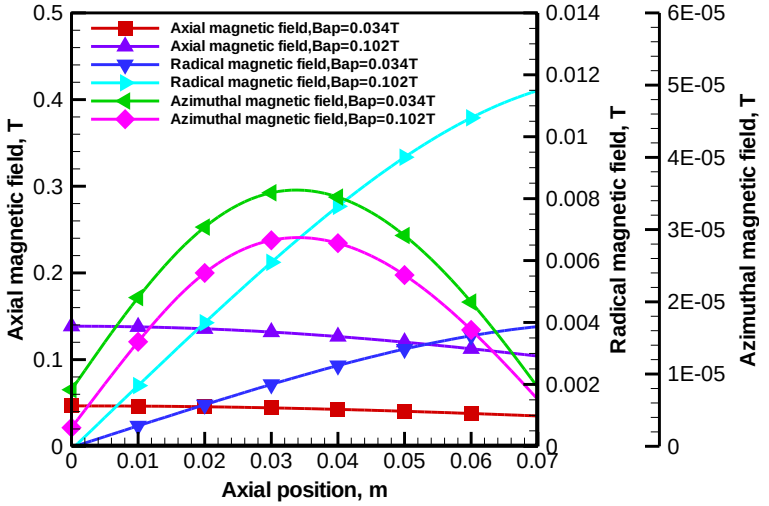

b) Thruster B

Figure 5. Axial variations of the magnetic field.

C. Thrust contributions of different acceleration mechanisms

As what have been discussed in section Ⅲ, dedicated thrust portions are attributed to different acceleration mechanisms in the AF-MPD thruster, and the thrust portion produced by each mechanism can be determined quantitatively by Eq. (17) - Eq. (20).

In this section, electromagnetic force density components resulting from different acceleration mechanisms, i.e., self-magnetic, Hall, and swirl modes are evaluated, and their distributions along the discharge channel for both thrusters under various applied magnetic field strengths are presented in Fig.8. The self-magnetic and Hall forces are much smaller than the swirl component and an increase of the applied field strength will increase the swirl component notably. Besides, the swirl component shows the tendency of having lower values at the entry and exit while reaching to a maximum value around the mid-point, which is similar to the distributions of the radical current density in Fig.7. This phenomenon is easy to understand: since the applied magnetic field strengths do not change much along the axial direction (slowing diverging as has be shown in Fig.5), the swirl component resulting from the applied magnetic field ($\boldsymbol{B}_z$, $\boldsymbol{B}_r$) and the discharge current ($\boldsymbol{j}_r$, $\boldsymbol{j}_z$) will vary substantially with the dominant discharge current component $\boldsymbol{j}_r$.

Table 4 presents thrust components resulting from the four acceleration modes with various applied field strengths for the mass flow rate of 0.1g/s and total discharge current of 1000A. We can conclude that swirl acceleration is the main thrust contributor in AF-MPD thrusters with parallel electrodes under the given operation conditions, and the thrust contributions of self-magnetic, Hall, gas-dynamic, and swirl acceleration mechanisms are in the approximate ratio of 1:10:10:100 in both of the two thrusters.

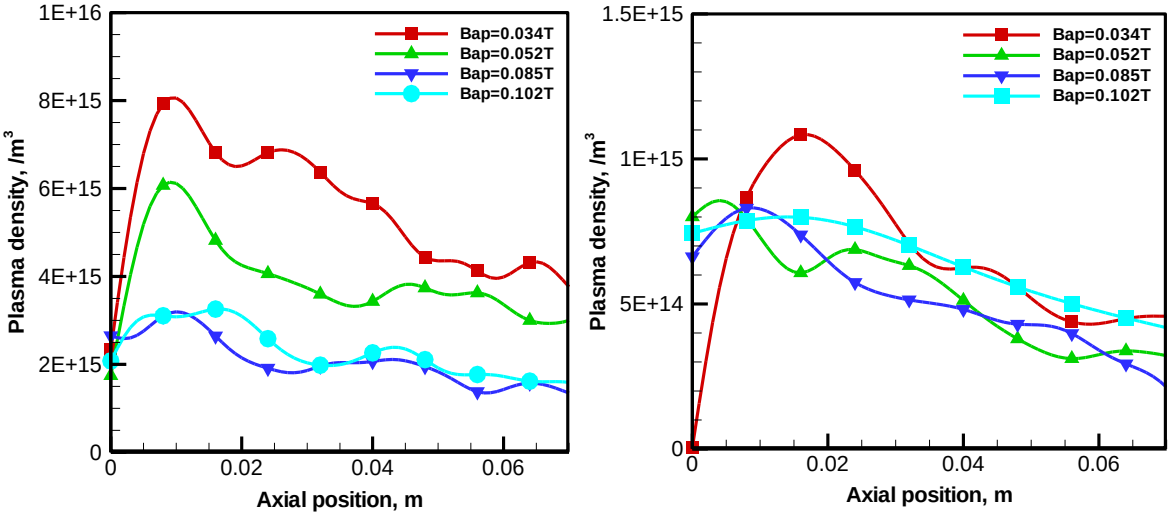

a) Thruster A **b) Thruster B**

Figure 6. Axial variations of plasma densities with different applied magnetic field strengths.

Besides, thrust components resulting from the electromagnetic acceleration mechanisms in the thruster with smaller anode radius (thruster A) are generally larger than those of thruster B, which may be attributed to the difference of the total ion qualities of the two thrusters. In fact, according to the analyses in Section B, more ions exist in thruster A under the given conditions so that the electromagnetic components can make more sense.

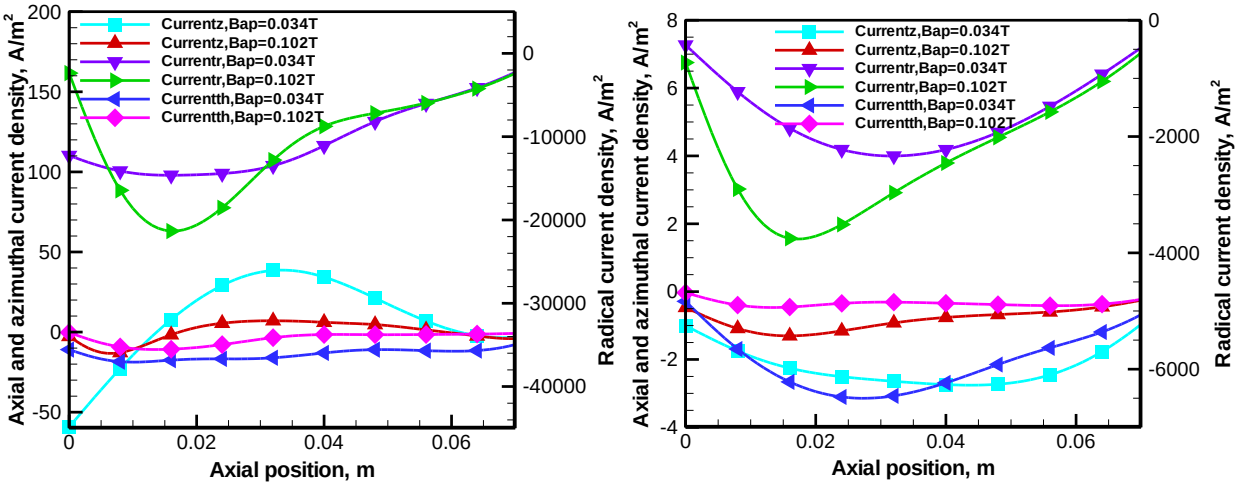

a) Thruster A **b) Thruster B**

Figure 7. Axial variations of current densities with different applied magnetic field strengths.

Furthermore, the gas-dynamic thrust components do not change much among the two thrusters under the same applied magnetic field strength. A bold speculation can be proposed that the anode shape of the thruster may have a notable effect on the gas-dynamic acceleration mechanism, e.g., thrusters with flared anodes may have larger gas-dynamic proportions than those with parallel electrodes under the same inlet dimensions and the same operation conditions, with the simple knowledge that the expansion shape can contribute to the energy conversions of the thermal energy to the useful axial kinetic energy in a physical nozzle. With this speculation in mind, the numerical simulation will be continued to investigate AF-MPD thrusters with various anode shapes, e.g., flared anode or converging-diverging anode under a wider applied magnetic field strength range.

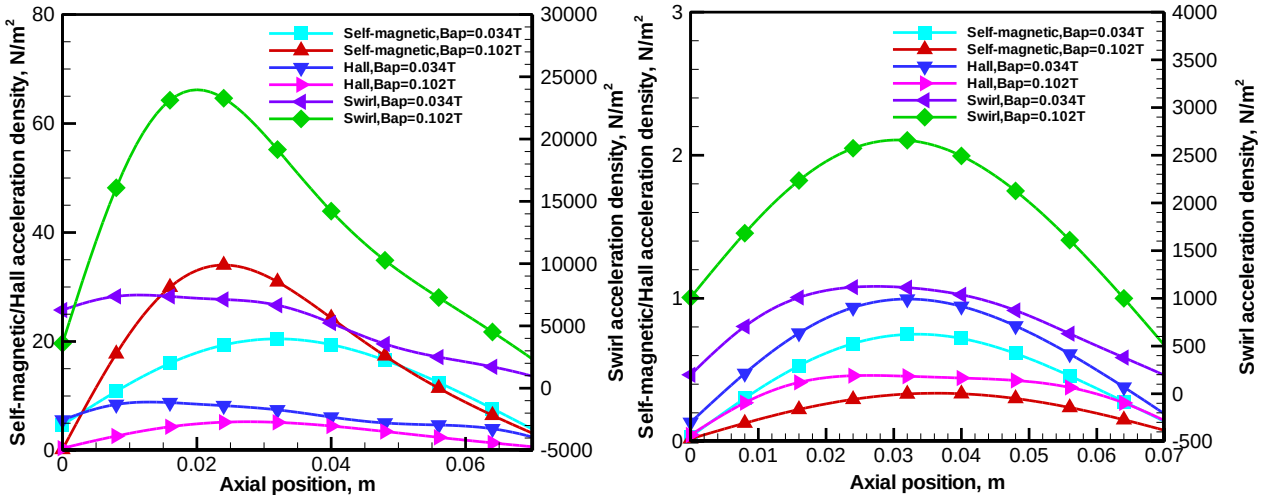

a) Thruster A **b) Thruster B**

Figure 8. Axial variations of electromagnetic forces with different applied magnetic field strengths.

Table 4. Average self-magnetic, Hall, swirl, and gas-dynamic acceleration contributions to thrust with various applied field strengths for mass flow rate of 0.1g/s and total discharge current of 1000A.

Thruster Geometry	Bap (T)	Self-magnetic (N)	Hall (N)	Swirl (N)	Gas-dynamic (N)
A	0.034	0.0055	0.0734	1.2214	0.0377
	0.052	0.0052	0.0684	2.1319	0.0694
	0.085	0.0042	0.0605	2.3766	0.1365
	0.102	0.0037	0.0558	2.5377	0.1927
B	0.034	0.0009	0.0369	0.8196	0.0434
	0.052	0.0008	0.0422	1.2859	0.0820
	0.085	0.0008	0.0573	1.7711	0.1218
	0.102	0.0007	0.0660	2.0122	0.1307

V. Conclusion

Two AF-MPD thrusters that are of different sizes and had been investigated experimentally by the NASA Lewis Research Center Group were simulated with the PIC-MCC method in this paper to obtain an insight into the geometric effects on the acceleration mechanisms in AF-MPD thrusters. Based on the characteristics of AF-MPD thrusters, the discharge chambers simulated were assumed to be axisymmetric and only electrons, single charged ions, and neutral atoms were taken into consideration. Besides, each plasma component was assumed to be two dimensional in space (z, r variation) and three dimensional in velocity in the simulation model and the applied magnetic field strength was varied from 0.034 T to 0.102 T with a mass flow rate of 0.1g/s and discharge current of 1000A.

Specific impulse variations with different applied magnetic field strengths were calculated for the two thrusters and compared with the experimental data. A good agreement was captured then, which helped verify the validity the simulation model. Based on the assumption that all types of nondirected energies can theoretically be converted into useful axial kinetic energy in the mechanical or the magnetic nozzle, delicate simulations on the thrust portion produced by each acceleration mechanism indicated that swirl acceleration mechanism was the dominant contributor to plasma acceleration, and self-magnetic, Hall, gas-dynamic, and swirl acceleration mechanisms were in an approximate ratio of 1:10:10:100. Besides, the total ion qualities and the thrust components resulting from the electromagnetic acceleration mechanisms tended to be larger in the thruster with smaller anode radius. In contrast to the electromagnetic thrust components, the gas-dynamic one did not change much among the two thrusters at the same applied magnetic field strength, which helped to conclude that the variations of the anode radii of AF-MPD thrusters would influence the electromagnetic acceleration mechanisms in the thrusters whereas had little impact on

the gas-dynamic acceleration mode. Finally, a bold speculation was proposed that the anode shape of the thruster may have a notable effect on the gas-dynamic acceleration mechanism. Future work will be focused on the simulations of AF-MPD thrusters with different anode shapes, e.g., flared anode or convergence-divergence anode under a wider applied magnetic field strength range to investigate these effects and shed more light on the optimum geometry design of AF-MPD thrusters.

Acknowledgments

This work was supported by National Science Foundation of China (No. 51276006) and Basic Scientific Research Foundation of Beihang University (No.YWF-13-D2-HT-12).

References

[1]Upadhyay, P. P., Herdrich, G., Petkow, D., Fasoulas, S., and Roser, H. P., "Numerical Simulation and Investigation of Self and Applied Field Magnetoplasmadynamic Thrusters for Argon Plasma," *47th AIAA/ASME/SAE/ASEE Joint Propulsion Conference & Exhibit*, AIAA, Washington, DC, 2011, AIAA 2011-6076.

[2]Tahara, H., Kagaya, Y., and Yoshikawa, T., "Performance and Acceleration Process of Quasisteady Magnetoplasmadynamic Arcjets with Applied Magnetic Fields," *Journal of Propulsion and Power*, Vol. 13, No. 5, 1997, pp. 651-658.

[3]Myers, R. M., "Scaling of 100 kW Class Applied-Field MPD Thrusters," *28th AIAA/ASME/SAE/ASEE Joint Propulsion Conference & Exhibit*, AIAA, Washington, DC, 1992, AIAA 92-3462.

[4]Tang, H. B., Cheng, J., and York, T.M., "Study of applied magnetic field magnetoplasmadynamic thrusters with particle-in-cell and Monte Carlo collision. II. Investigation of acceleration mechanisms," *Physics of Plasmas*, Vol. 19, 2012, pp. 1-11.

[5]Paganucci, F., Rossetti, P., Andrenucci, M., Tikhonov, V. B., and Obukhov, V. A., "Performance of an Applied Field MPD Thruster with a Pre-ionization Chamber," *33rd Plasmadynamics and Lasers Conference*, AIAA, Washington, DC, 2002, AIAA 2002-2103.

[6]Kodys, A. D. and Choueiri, E. Y., "A Critical Review of the State-of-the-Art in the Performance of Applied-Field Magnetoplasmadynamic Thrusters," *41st AIAA/ASME/SAE/ASEE Joint Propulsion Conference & Exhibit*, AIAA, Washington, DC, 2005, AIAA 2005-4247.

[7]Myers, R. M., "Applied-Field MPD Thruster Performance with Hydrogen and Argon Propellants," *J. Propulsion*, Vol. 9, No. 5, 1993, pp. 781-784.

[8]Mikellides, P. G., and Turchi, P. J., "Applied-Field Magnetoplasmadynamic Thrusters, Part 1: Numerical Simulations Using the MACH2 Code," *Journal of Propulsion and Power*, Vol. 16, No. 5, 2000, pp. 887-893.

[9]Sasoh, A. and Arakawa, Y., "Electromagnetic Effects in an Applied-Field Magnetoplasmadynamic Thruster," *J. Propulsion*, Vol. 8 No. 1, 1990, pp. 98-102.

[10]Sasoh, A., "Simple Formulation of Magnetoplasmadynamic Acceleration," *Physics of Plasmas*, Vol. 1, No. 3, 1994, pp. 464-469.

[11]Tahara, H., Sasaki, M., Kagaya, Y., and Yoshikawa, T., "Thruster Performance and Acceleration Mechanisms of a Quasi-steady Applied-field MPD Arcjet," *AIAA/DGLR/JSASS 21st International Electric Propulsion Conference*, AIAA, Washington, DC, 1990, AIAA 90-2554.

[12]Sasoh, A., "Thrust Formula for Applied-Field Magnetoplasmadynamic Thrusters Derived from Energy Conservation Equation," *Journal of Propulsion and Power*, Vol. 11, No. 2, 1995, pp. 351-356.

[13]Krulle, G., Auwerter-Kurtz, M., and Sasoh, A., "Technology and Application Aspects of Applied Field," *Journal of Propulsion and Power*, Vol. 14, No. 5, 1998, pp. 754-763.

[14]Myers, R. M., "Applied-Field MPD Thruster Geometry Effects," *27th AIAA/ASME/SAE/ASEE Joint Propulsion Conference & Exhibit*, AIAA, Washington, DC, 1991, AIAA 1991-2342.

[15]Mantenieks, M. A., Sovey, J. S., Baag, T. W., and Raitano, P., "Performance of A 100kW Class Applied Field MPD Thruster," *25th AIAA/ASME/SAE/ASEE Joint Propulsion Conference & Exhibit*, AIAA, Washington, DC, 1989, AIAA 89-2710.

[16]Myers, R. M., Mantenieks, M. A., and Sovey, J. S., "Geometric Effects in Applied-Field MPD Thrusters," *AIAA/DGLR/JSASS 21st International Electric Propulsion Conference*, AIAA, Washington, DC, 1990, AIAA 90-2669.

[17]Myers, R. M., "Geometric Scaling of Applied-Field Magnetoplasmadynamic Thrusters," *Journal of Propulsion and Power*, Vol. 11, No. 2, 1995, pp. 343-350.

[18]Takubo, M., Koizumi, H., Hyakutake, T. and Kuninaka, H., "Effect of Inter-electrode Geometry on the Performance of an Applied-Field 2D MPD Thruster," *48th AIAA/ASME/SAE/ASEE Joint Propulsion Conference & Exhibit*, AIAA, Washington, DC, 2012, AIAA 2012-4013.

[19]Boxberger, A., Bambach, P., Herdrich, G. and Fasoulas, S., "Experimental Investigation of Steady-State Applied-Field Magnetoplasmadynamic Thrusters at Institute of Space Systems," *48th AIAA/ASME/SAE/ASEE Joint Propulsion Conference & Exhibit*, AIAA, Washington, DC, 2012, AIAA 2012-4012.

[20]Sankaran, K., Choueiri, E. Y., and Jardin, S.C., "Comparison of Simulated Magnetoplasmadynamic Thruster Flowfields to Experimental Measurements," *Journal of Propulsion and Power*, Vol. 21, No. 1, 2005, pp. 129-138.

[21]Sleziona, P. C., Auwerter-Kurtz, M., Schrade, H. O., and Wegmann, T., "Comparison of Numerical and Experimental Investigations of Nozzle Type MPD Accelerators," *AIAA/DGLR/JSASS 21st International Electric Propulsion Conference*, AIAA, Washington, DC, 1990, AIAA 90-2663.

[22]Mikellides, P. G., and Turchi, P. J., "Applied-Field Magnetoplasmadynamic Thrusters, Part 2: Analytic Expressions for Thrust and Voltage," *Journal of Propulsion and Power*, Vol. 16, No. 5, 2000, pp. 894-901.

[23]Adam, J. C., Heron, A., and Laval, G., "Study of Stationary Plasma Thrusters Using Two-Dimensional Fully Kinetic Simulations," *Physics of Plasmas*, Vol. 11, No. 1, 2004, pp. 295-305.

[24]Boulanger, L., Pang, A., Raitses, Y. and Martinez-Sanchez, M., "Validation of Fully-Kinetic Particle-in-Cell Model Optimized for Multi-Thruster Adaptability," *49th AIAA/ASME/SAE/ASEE Joint Propulsion Conference & Exhibit*, AIAA, Washington, DC, 2013, AIAA 2013-3886.

[25]Marshall, D. D., and VanGilder, D. B., "Investigation of Particle-in-Cell Acceleration Techniques for Plasma Simulations," *37th AIAA Plasmadynamics and Lasers Conference*, AIAA, Washington, DC, 2006, AIAA 2006-3248.

[26]Mahalingam, S., "Particle Based Plasma Simulation for an Ion Engine Discharge Chamber," Ph.D. Dissertation, Mechanical and Materials Engineering Dept., Wright State Univ., Fairborn, OH, 2007.

[27]McDonald, M. S., "Electron Transport in Hall Thrusters," Ph.D. Dissertation, Aerospace Engineering Dept., Michigan Univ., Ann Arbor, MI, 2012.

[28]Fox, J. M., "Advances in Fully-Kinetic PIC Simulations of a Near-Vacuum Hall Thruster and Other Plasma Systems," Ph.D. Dissertation, Aeronautics and Astronautics Dept., Massachusetts Institute of Technology, Cambridge, MA, 2007.

[29]Parra, F. I., and Ahedo, E., "A two-dimensional hybrid model of the Hall thruster discharge," *Physics of Plasmas*, Vol. 100, 2006, pp. 1-11.

[30]Wirz, R. E., "Discharge Plasma Processes of Ring-Cusp Ion Thrusters," Ph.D. Dissertation, Aerospace Dept., California Institute of Technology, Pasadena, CA, 2005.

[31]Cheng, S. Y. M., "Modeling of Hall thruster lifetime and erosion mechanisms," Ph.D. Dissertation, Aeronautics and Astronautics Dept., Massachusetts Institute of Technology, Cambridge, MA, 2007.

[32]Tang, H. B., Cheng, J., and York, T.M., "Study of applied magnetic field magnetoplasmadynamic thrusters with particle-in-cell and Monte Carlo collision. I. Computation methods and physical processes," *Physics of Plasmas*, Vol. 19, 2012, pp. 1-11.

[33]Szabo, J. J., "Fully Kinetic Numerical Modeling of a Plasma Thruster," Ph.D. Dissertation, Aeronautics and Astronautics Dept., Massachusetts Institute of Technology, Cambridge, MA, 2001.

[34]Wang, J., Liewer, P. C., and Huang, E., "3D Electromagnetic Monte Carlo Particle-in-Cell Simulations on MIMD Parallel Computers," *33rd Aerospace Sciences Meeting and Exhibit*, AIAA, Washington, DC, 1995, AIAA 95-0593.

[35]Myers, R. M., Mantenieks, M. A., and Lapointe, M. R., "MPD Thruster Technology," *AIAA/NASA/OAI Conference on Advanced SEI Technologies*, AIAA, Washington, DC, 1991, AIAA 91-3568.